Hydrogen Bonding and its Effect on the Orientational Dynamics of Water Molecules inside Polyelectrolyte Brush-Induced Soft and Active Nanoconfinement

Harnoor Singh Sachar, Bhargav Sai Chava, Turash Haque Pial, and Siddhartha Dasa,*

^aDepartment of Mechanical Engineering, University of Maryland, College Park, MD 20742,

United States

*sidd@umd.edu

Abstract

Despite being the most ubiquitous compound on Earth, the fundamental properties of water are not fully understood, especially in nanoconfinement. Densely grafted polyelectrolyte (PE) molecules attain the configuration of a "brush": these PE brushes, due to their ability to form hydrogen bonds (HBs) with water via the PE functional groups, act as a source of soft and active nanoconfinement for the brush-trapped water molecules. In this paper, we study the effects of PE brush-induced confinement on the structure, dynamics and energetics of the water-water and water-PE HBs. Our results indicate a significant weakening of the HBs from bulk to sparsely grafted to densely grafted brushes. i.e., by increasing the degree of brush-induced nanoconfinement. We explain that this weakening of water-water HBs is caused by the disruption of the extended network of water molecules within the brush-induced nanoconfinement. This is confirmed by performing a ring structure analysis of the water molecules, which yields a reduction in the average ring size at higher degrees of brush-induced nanoconfinement (i.e., at higher brush grafting densities). Furthermore, we investigate the role of HB on the orientational dynamics of the water molecules. We observe that the rotational motion of the water molecules becomes sluggish inside the PE brushes. Recent findings have indicated that the water and counterions trapped in brush-induced nanoconfinement demonstrate structures (in combination with the PE functional group) analogous to that in "water-in-salt" electrolytes that have seen extensive recent uses for Li-ion battery applications. However, the rotational dynamics of water molecules inside the brush-induced nanoconfinement is found to be distinctly different from that of conventional "water-in-salt" electrolytes in absence of any confinement; therefore, the present study will provide the necessary platform towards conceptualizing polymer-based nanoconfinement for battery applications.

Introduction

Polyelectrolyte (PE) molecules grafted on a substrate in close proximity to each other swell to form "brush"-like configurations. PE brush coatings have been employed in various applications ranging from fabrication of nanofluidic energy conversion devices¹⁻² and current rectifiers³⁻⁴, stabilization of emulsions⁵ to targeted drug delivery⁶⁻⁷ and oil recovery⁸. There has been extensive research on the overall structure and configuration of PE brushes over the past few decades. However, a comprehensive understanding of several fundamental phenomena such as the hydrogen bond (HB) network, counterion solvation structure, and local arrangement of water molecules within the PE brushes is lacking. There have been some recent advances in our understanding of the microstructure of PE brushes through investigations by the Das group⁹⁻¹⁰ that employed all-atom molecular dynamics (MD) simulations to probe the structure and properties of PE brushes as well as the brush-supported counterions and water molecules. Such insights into the atomistic-scale details are critical not only to develop novel uses for PE brush systems but also to improve the efficiency of several existing applications.

In this study, we employ fully atomistic MD simulations to probe the structure, energetics, and dynamics of hydrogen bonds (HBs) in the nanoconfinement enforced within the water-swollen densely grafted PE brushes. Our previous study has revealed that such densely grafted PE brushes enforced a significant nanoconfinement effect and massively reduced the mobility of the water molecules and the screening counterions. Charges on the PE chains render water, having a high dielectric constant, a typical good solvent for the PE brushes. A recent experimental study revealed that hydrogen bonding plays a pivotal role in dictating the swelling behavior of water-swollen polymer brushes such as poly(2,5-dimethoxyaniline) (PDMA), poly(oligo[ethylene glycol] methyl ether methacrylate) (POEGMA), poly(2-[2-methoxyethoxy]ethyl methacrylate) (PMEO₂MA),

etc.¹¹ However, the experiments did not provide an atomistic picture of the underlying changes in the strength and dynamics of the HBs. On the theoretical front, Szleifer and coworkers published a study that accounted for the effect of water-water and water-polymer HBs on the configuration of poly(ethylene oxide) (PEO).¹² Ref. 12 is based on the formulation first proposed by Dormidontova (Ref. 13), where the author studied the effect of water-PEO and water-water HBs in the behavior of PEO molecules in an aqueous solution. In this theoretical framework, the free energy change associated with the formation of the water-water and water-PEO HBs has been expressed as functions of the ΔE_w (the energetic gain associated with the formation of a single water-water HB), ΔE_p (the energetic gain associated with the formation of a single water-PEO HB), and ΔS_i [the dimensionless entropy change associated with the formation of the water-water HB (i=w) and water-PEO HB (i=p)]. In both these studies, ΔE_w , ΔE_p , ΔS_w , and ΔS_p are assumed to be constant (i.e., independent of the concentration of the PEO in Ref. 13 and independent of the presence of the brushes or the brush grafting density in Ref. 12). A constancy in ΔE_i and ΔS_i will imply a constancy in the corresponding free energy change ΔF_i , where $\Delta F_i = \Delta E_i - kT\Delta S_i$ (k and T denote the Boltzmann constant and temperature respectively). Our simulations will test the validity of such an assumption where the change in free energy ΔF_i associated with the formation of a single water-water HB (i = w) or with the formation of a single water-polymer HB (i = p) is assumed to be independent of the polymer concentration (or the polymer brush grafting density). This will be done by quantifying the water-water and water-PE HB strength for different PE brush grafting densities (or equivalently, the different extents of confinement enforced by the densely grafted PE brushes). Finally, we will study the consequences of change in HB network inside the brushes on the rotational dynamics of the PE brush-supported water molecules.

Our results indicate a significant decrease in the water-water and water-PE HB strength with an increase in the degree of PE brush-induced soft confinement (quantified by the grafting density of the brushes). Interestingly, in the context of the hydrogen bonding, the confinement enforced by the PE brushes serves as an "active" confinement since the PE brushes that form the confinement themselves take part in the HB formation. We link the weakening of the strength of the water-water HBs inside the brush-induced confinement to a decrease in the extensive HB network formed by the (brush-supported) water molecules as evident from their ring structure analysis. Furthermore, we observe that for our system the water-PE HBs are more stable than the water-water HBs from both an energetic and a dynamics standpoint. We proceed to show that the stability of water-PE HBs plays a critical role in ensuring that the orientational dynamics of water becomes sluggish inside densely grafted PE brushes. More importantly, this water orientational dynamics inside the brush-induced nanoconfinement is remarkably different from the rotational behavior of water molecules in conventional "water-in-salt" electrolyte systems in the absence of nanoconfinement. Such "water-in-salt" systems refer to the system of highly concentrated aqueous solutions (where the salt overwhelms water by both mass and volume)¹⁴ that have found massive recent applications in Li-ion batteries: interestingly, our recent paper (Ref. 9) has shown that the structure of the water and the screening counterions trapped inside the densely grafted PE brush layer (or the PE-brush-induced nanoconfinement), along with the charged functional groups of the PE brushes, become analogous to the water-ion structure in bulk "water-in-salt" electrolyte systems. Therefore, this dissimilarity in the water orientational dynamics within the PE brush induced nanoconfinement, as compared to that for the standard (without confinement) "water-insalt" systems point to the importance of the present study in developing the foundation of PEbrush-driven soft and active nanoconfinement for possible battery applications.

Results and Discussions

Our system contains 36 fully ionized polyacrylic acid (PAA) chains, grafted on the plane z=0 in a 6x6 square array (see Fig. 1). The chains are monodispersed with each containing 49 backbone Carbon atoms. Our simulations probe the effect of two different grafting densities, $\sigma_g = 0.1/\sigma^2$, $0.2/\sigma^2$ [where $\sigma = 3.5$ Å is the distance corresponding to zero Lennard-Jones (LJ) interaction energy between the backbone Carbon atoms]. The charge on the brushes are neutralized by adding appropriate number of Na⁺ counterions. SPC/E water molecules act as the explicit solvent for the brushes. ¹⁵ Further details regarding the simulation procedure are provided in in the Methods section.

Effect of PE brush-induced confinement on hydrogen bond strength

We start by quantifying the effect of brush grafting density, which dictates the extent of PE brush induced nanoconfinement, on the strength of water-water and water-PE HBs. A water molecule can act as a HB donor to other water molecules serving as acceptor (leading to the formation of water-water HBs) as well as the Oxygen atoms (which then serve as acceptor) on the Carboxylate groups of PAA chains (leading to the formation of water-PE HBs). The HB strength (for both water-water and water-PE HBs) is calculated using the methodology of Sapir and Harries, ¹⁶ who defined the HB energy as the reversible work done to orient an ensemble of donor and acceptor pairs in their equilibrium probability distribution $P(r,\theta)$ from a state of random distribution $P_{rand}(r,\theta)$. Here, r and θ represent the distance between donor and acceptor Oxygens and the angle formed by the Hydrogen-(donor Oxygen)-(acceptor Oxygen) triad, respectively. A detailed description of the HB strength calculations can be found in the Methods section.

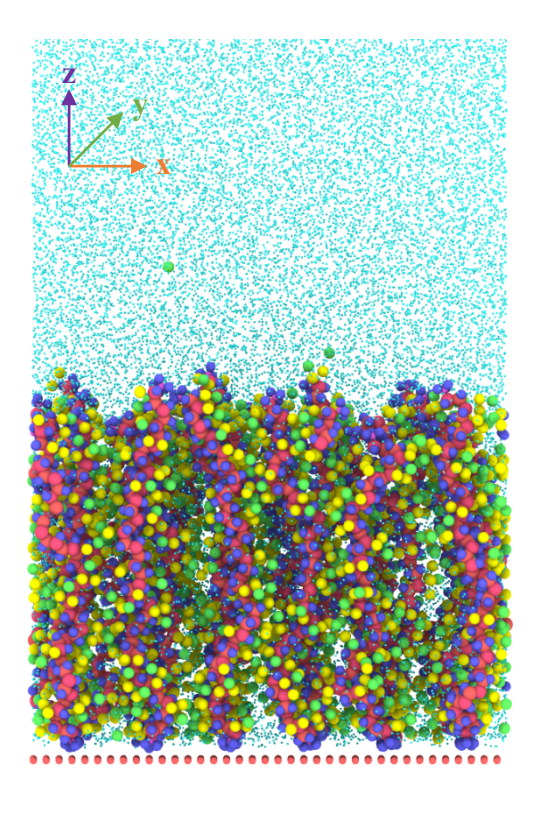


Figure 1: Snapshot (truncated from the top) of the simulation domain for $\sigma_g = 0.1/\sigma^2$. Particle sizes are scaled to their Lennard Jones (LJ) diameters, except for water molecules (in order to improve visualization). Green particles represent the Na⁺ counterions, red particles represent the discrete repulsive wall while other colors represent various atom types of the PAA molecules.

Table 1 lists the Gibbs free energy (ΔG) associated with the formation of water-water HBs (in bulk and inside the brushes). We observe a significant decrease in the water-water HB strength inside the brushes, as quantified by a decrease in the magnitude of ΔG . In addition, the reduction in the bond strength is more pronounced at higher grafting densities. Thus, the water-water HBs become weaker as the extent of the PE brush-induced nanoconfinement is increased (caused by an increase in the PE brush grafting density). This is the most important finding of this article. Prior studies have also reported a decrease in hydrogen bond strength in several nanoconfined systems, 17-21 albeit not for the case of polymer/PE brush-indued confinement. The second critical facet of this study is the fact that the PE brushes act as a form of soft and active nanoconfinement, where the source of the confinement itself forms hydrogen bonds with the water molecules. Thus, they are fundamentally different from (and much more complex than) other forms of passive nanoconfinement such as graphene sheets, carbon nanotubes, etc. which only act as physical barriers but do not participate in hydrogen bonding with the confined species themselves. To understand the decrease in water-water HB strength, we plot the joint probability density $[P(r, \theta)]$ of the water-water donor-acceptor pairs in Figure 2(b-d). Figure 2(a) depicts the random joint probability distribution $[P_{rand}(r,\theta)]$ associated with the donor-acceptor pairs in bulk water. This distribution remains (almost) the same even for water molecules trapped inside the PE brushes [see Fig. S3 in the Supporting Information (SI)]. We observe that the joint probability distribution for bulk water [see Fig. 2(b)] has only one basin within the cutoffs for hydrogen bond formation 2.45~Å < r < 3.35~Å [cutoffs are depicted by horizontal dashed white lines in Fig. 2(b-d)]. This basin is concentrated around r=2.7 Å, θ =10°. Water molecules separated by a distance r greater than the maximum cutoff value (3.35 Å) represent the second solvation shell and do not participate in hydrogen bonding. Procedure for obtaining the cutoffs is provided in the Hydrogen Bond

Strength Calculation subsection of the Methods section. Inside the brushes, we see that a second basin centered around θ =50° becomes increasingly prominent within the cutoff region for r. This is especially true for brushes with high grafting density ($\sigma_g = 0.2/\sigma^2$). Thus, at higher grafting densities, the distribution of θ values become broader and is no longer confined to small values. As a result, the joint probability distribution [$P(r,\theta)$] starts to bear a closer resemblance to the random joint probability distribution [$P_{rand}(r,\theta)$], which peaks around θ =45° for a given value of r [$P_{rand}(r,\theta) = 4\pi r^2 P_{rand}(\theta)$, where $P_{rand}(\theta)$ is the angular distribution associated with the donor Hydrogen-(donor Oxygen)-(acceptor Oxygen) triads¹⁶]. This reduces the amount of work required to reorient the water molecules from a state of random distribution to their equilibrium probability distribution and hence reduces the HB strength at higher degrees of brush-induced confinement.

Donor-Acceptor Pair	Environment	ΔG (kJ/mol)
Water-Water	Bulk	-3.27
Water-Water	Inside brushes ($\sigma_g = 0.1/\sigma^2$)	-2.42
Water-Water	Inside brushes ($\sigma_g = 0.2/\sigma^2$)	-1.90
Water-PE	Inside brushes ($\sigma_g = 0.1/\sigma^2$)	-4.55
Water-PE	Inside brushes ($\sigma_g = 0.2/\sigma^2$)	-3.63

Table 1: Gibbs free energy (Δ G) of formation of water-water and water-PE hydrogen bonds in various environments.

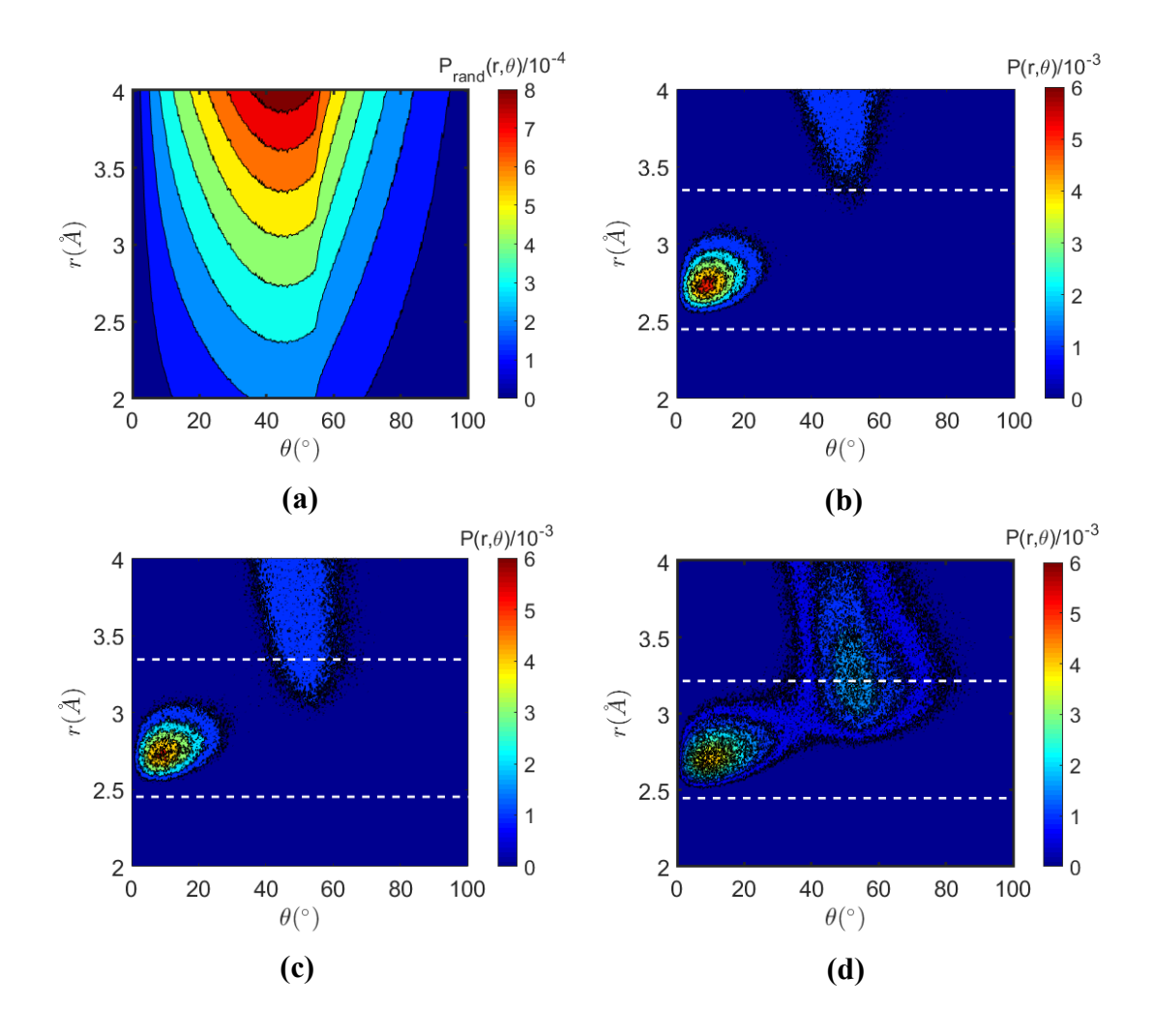


Figure 2: Contours of (a) $P_{rand}(r,\theta)$ and (b) $P(r,\theta)$ for water-water donor-acceptor pairs in bulk water. (c) and (d) depict the contours of $P(r,\theta)$ for water-water donor-acceptor pairs inside PE brushes with $\sigma_g = 0.1/\sigma^2$ and $\sigma_g = 0.2/\sigma^2$ respectively. The cutoffs for hydrogen bond formation in (b), (c) and (d) are depicted by horizontal dashed white lines.

In an attempt to paint a physical picture for the weakening of water-water HBs inside the PE brushes, we explore the network topology of the water molecules. It is well known that water molecules form an extensive network with each other as a result of their hydrogen bonding. 22-26 This network of HBs plays a vital role in dictating several important properties of liquid water such as the mass density and the rotational dynamics. ²⁷⁻³⁰ One commonly used tool to characterize the network topology of water molecules is the 'ring structure' analysis. ^{22-26, 31} Water molecules form a number of rings (or closed loops) due to the arrangement of HBs in a cyclic fashion [see Fig. 3(a)]. In Fig. 3(b), we plot the probability distribution [P(n)] as a function of the ring size (n)for water molecules inside the PE brushes and compare it to that of bulk water. For the purpose of this calculation as well as any subsequent analysis, we define the existence of a HB (water-water or water-PE) through the following geometric criteria: the interatomic distance between the donor and acceptor Oxygens, r < 3.5 Å and the angle formed by the Hydrogen-(donor Oxygen)-(acceptor Oxygen) triad, $\theta < 30^{\circ}$. ^{14,32-33} Note that this definition does not consider the contributions from the second basin (centered around θ =50°) within the cutoffs for HB formation, that becomes specially prominent for water-water donor-acceptor pairs inside the PE brushes with high grafting density [see Fig. 2(b-d)]. Prior studies have revealed that these HBs, associated with the second basin, are highly distorted and therefore we ignore them intentionally in our analysis.³⁴⁻³⁵ We set a maximum ring size of n=10 for our 'ring structure' calculations. Moreover, we only consider primitive rings (no pair of constituent molecules of the ring are connected by a HB path shorter than the path along the ring) in our analysis. 36-37 The detailed procedure for calculating the probability distribution of ring size is provided in the Methods section. Our results indicate a monotonic reduction in the probability of occurrence of larger rings (larger values of n) as one moves from bulk water to sparsely grafted brushes to densely grafted brushes. On the other hand, the share of smaller rings

(lower values of n) is enhanced inside the densely grafted brushes. This is consistent with the fact that larger rings are correlated to higher densities of water³⁸ (in a prior publication, we showed that the mass density of water decreases with an increase in grafting density of the brushes⁹). A shift towards the smaller ring sizes, in addition to the lowering of total number of rings normalized by the number of water molecules (see Table 2 for the ring statistics), indicates that the extended network of water molecules gets disrupted due to the nanoconfinement created by the brushes. The cooperative nature of HB leads to a two-way coupling between the network topology of water molecules (a global phenomenon) and the water-water HB strength (a local phenomenon), i.e., stronger HBs lead to a more extended network and vice versa. Therefore, the PE brush-induced nanoconfinement driven disruption of the large-scale network of water molecules (as quantified by the ring analysis) manifests in the form of weakened water-water HBs inside the brushes. A similar explanation was proposed by Wurpel and Müller for the reduction of HB strength in water confined between lipid bilayers.²⁰

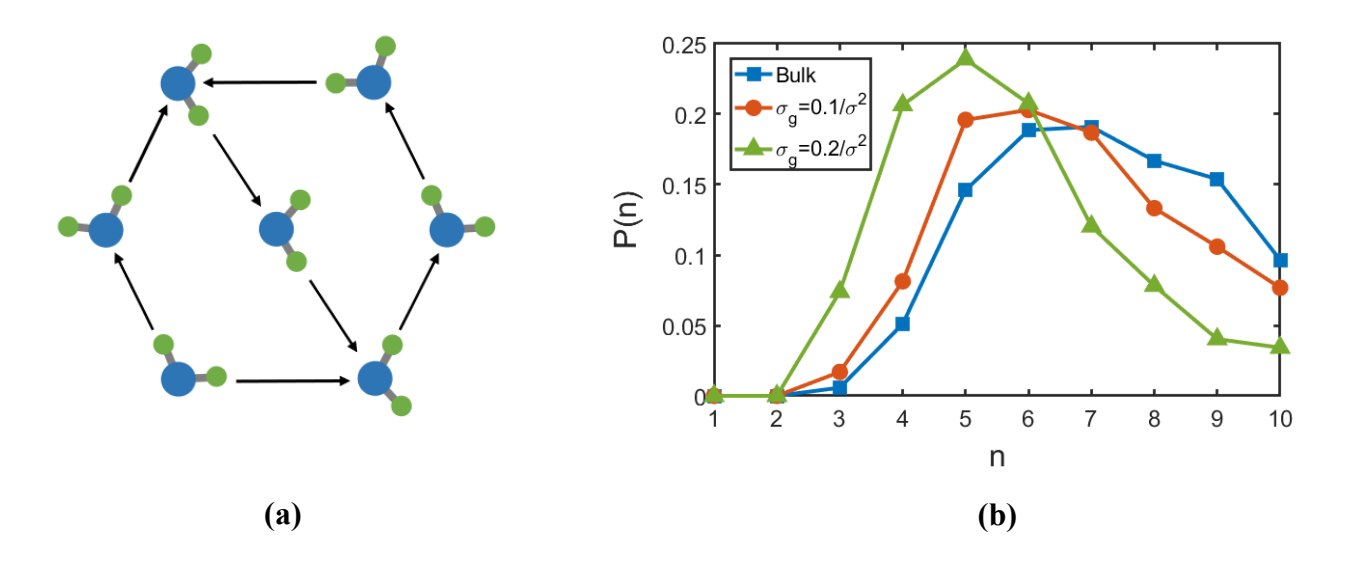


Figure 3: (a) Schematic representation of the ring structures formed by the water molecules. We can identify one hexagonal ring and two pentagonal rings in the given diagram. However, only the two pentagonal rings are counted as primitive rings. (b) Probability distribution [P(n)] of ring sizes (n) formed by water molecules trapped inside the PE brushes of different grafting densities. Ring size distribution for bulk water is also plotted for comparison.

Environment	Average ring size <n></n>	Number of rings normalized
		by number of water molecules
Bulk	7.11	1.97
Inside brushes ($\sigma_g = 0.1/\sigma^2$)	6.67	0.64
Inside brushes ($\sigma_g = 0.2/\sigma^2$)	5.66	0.10

Table 2: Ring statistics for bulk water and water molecules trapped inside PE brushes of different grafting densities.

We next study the water-PE HB strength within the brushes (see Table 1). We observe that the water-PE HBs are stronger (as quantified by a higher magnitude of $|\Delta G|$) than the water-water HBs at a given grafting density. Of course, this is not a generic result and depends on the choice of the PE molecules, especially from an enthalpic point of view. However, there is a fundamental difference between water-water and water-PE HBs that needs to be understood. PE functional groups are tethered to the backbone of the PE chains which greatly reduces their mobility. Thus, the O_{Carboxylate} atoms (Oxygen atoms on the Carboxylate groups of PAA chains) do not lose significant entropy upon the formation of HBs with the water molecules. This reduces the entropy loss associated with formation of the water-PE HBs and makes these HBs more stable in comparison to water-water HBs where both the species are mobile. We also witness a decrease in the bond strength, $|\Delta G|$ of water-PE HBs with an increase in grafting density of the brushes. The reasoning remains similar to the case of water-water HBs with the joint probability distribution $[P(r,\theta)]$ shifting towards higher values of θ within the cutoff values for r (see Figures 4 and S3 for the contour plots corresponding to the joint probability distribution and random joint probability density of water-PE pairs). Thus, lesser work is required to reorient the water-PE donor-acceptor pairs from a state of random distribution to their equilibrium probability distribution inside the brushes, thereby reducing the HB strength at higher degrees of brushinduced confinement.

We conclude this section with a brief discussion of the effect of degree of ionization of the PE chains (ratio of the number of charged monomers to the total number of monomers) on the water-water and water-PE HB strength. Up to this point, the PAA brushes were considered to be fully ionized. However, PAA is a weak polyacid and its degree of ionization depends on a number of factors such as the solution pH, grafting density, concentration of added salt, etc. The protonated

and deprotonated monomers interact differently with the water molecules, thereby affecting the number and strength of the water-PE HBs, and indirectly the number and strength of the waterwater HBs inside the brushes. In a prior publication, 10 we had reported a decrease in the number of water-water HBs (per water molecule) and an increase in the number of water-PE HBs (per PAA chain) within the brushes with an increase in the degree of ionization of the PAA chains. This trend suggests (but does not prove) a likely decrease in the water-water HB strength and an increase in the water-PE HB strength with an increase in the degree of ionization of the PAA chains. The increase in water-PE HB strength with degree of ionization makes intuitive sense since the deprotonated carboxylate groups (COO-) bear a full negative charge as opposed to the protonated carboxylic acid groups (COOH), which are neutral as a whole. Thus, hydrogen bonding between the water molecules and COO groups would be enthalpically more favorable than that between water and COOH groups. On the other hand, the decrease in water-water HB strength with an increase in the degree of ionization is not as apparent. To verify if this is indeed the case, we calculated the water-water HB strength inside fully protonated PAA brushes using the methodology of Sapir and Harries. 16 In line with expectation, our results indicate a higher waterwater HB strength inside the fully protonated brushes ($\sigma_g = 0.1/\sigma^2$: $\Delta G = -3.13$ kJ/mol, $\sigma_g =$ $0.2/\sigma^2$: $\Delta G = -2.96$ kJ/mol) as compared to the fully ionized PE brushes ($\sigma_g = 0.1/\sigma^2$: $\Delta G = -0.1/\sigma^2$ 2.42 kJ/mol, $\sigma_g = 0.2/\sigma^2$: $\Delta G = -1.90$ kJ/mol).

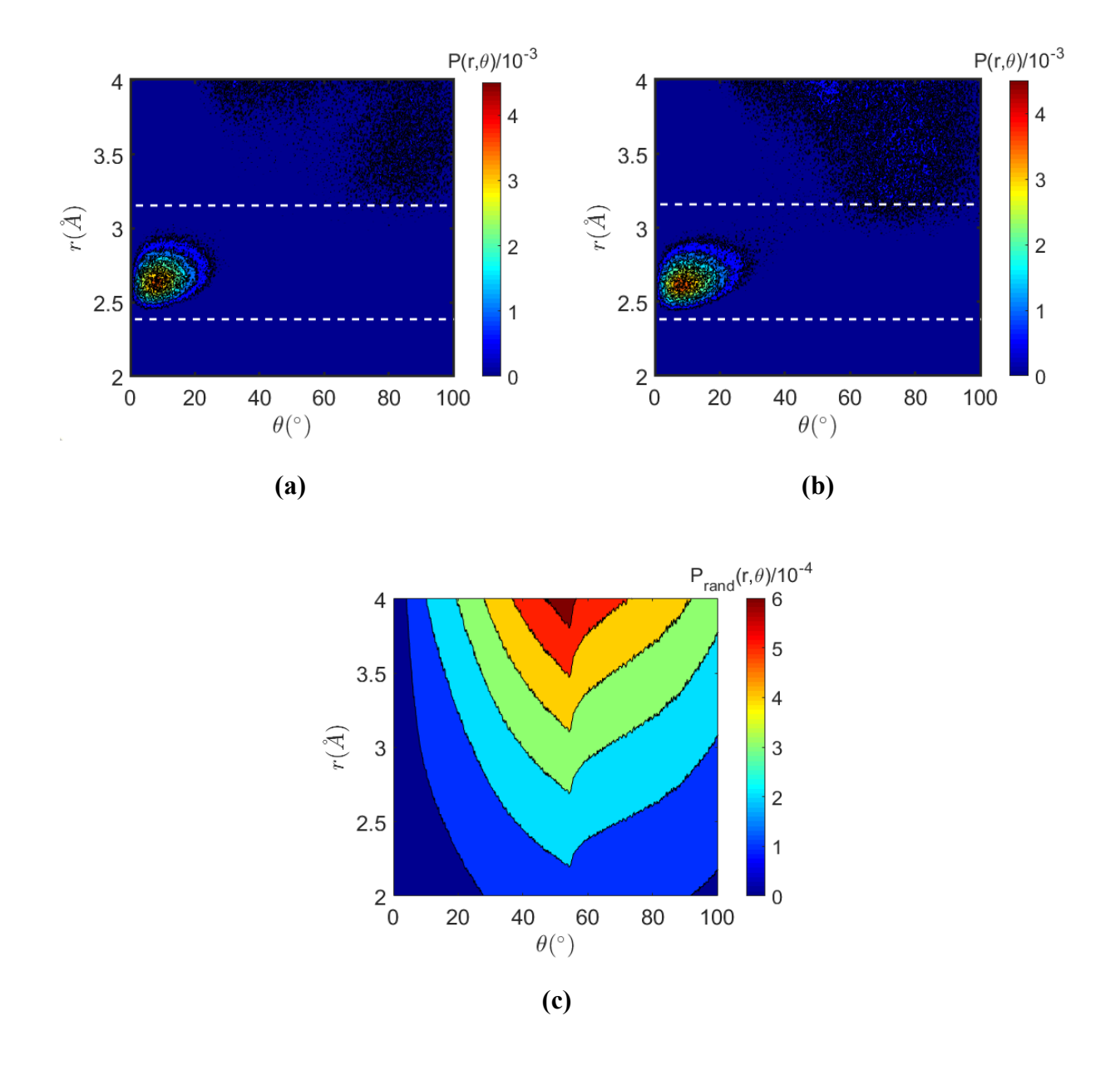


Figure 4: (a) and (b) depict the contours of $P(r,\theta)$ for water-PE donor-acceptor pairs inside the PE brushes with $\sigma_{\rm g}=0.1/\sigma^2$ and $\sigma_{\rm g}=0.2/\sigma^2$ respectively. (c) Contours of $P_{rand}(r,\theta)$ for water-PE donor-acceptor pairs inside PE brushes with $\sigma_{\rm g}=0.1/\sigma^2$. The cutoffs for hydrogen bond formation in (a) and (b) are depicted by horizontal white dashed lines.

Orientational dynamics of water inside the PE brushes

Recently, Zhang and coworkers showed that a solid-state aqueous polymer electrolyte (SAPE) consisting of a "water-in-salt" solution (highly concentrated aqueous solution where the salt overwhelms water by both mass and volume) inside a polymer matrix helped increase the stability-window for Li-ion batteries.³⁹ The high affinity of the water molecules for the hydrophilic polymer network slows down their motion and helps decrease the rate of decomposition of the water molecules at the anode, thereby increasing the overall electrochemical stability of the battery. Keeping this in mind, it is extremely important to not only study the dynamics of water molecules in polymer based "water-in-salt" systems but also compare their behavior to conventional "water-in-salt" electrolytes, that have been at the forefront of Li-ion battery research for the past few years. 40-42 In a prior publication, we had shown that the translational mean squared displacement of water molecules decreases monotonically with increasing degree of PE brushinduced nanoconfinement (from 'bulk' to 'sparsely grafted PE brushes' to 'densely grafted PE brushes'). In this section, we investigate the role of hydrogen bonding in dictating the rotational dynamics of the PE brush-trapped water molecules, as quantified by their rotational mean squared displacement (RMSD). The orientational properties of water molecules are critical to many processes involving proton transfer, 43-44 protein hydration, 45 etc. Three principal directions (axes) are needed to fully describe the rotational motion of a water molecule. Following the notation of Han, ¹⁴ we choose the three axes as follows [see Fig. 5(a)]:

 \vec{H} – Unit vector connecting the Oxygen atom to the midpoint of the Hydrogen atoms (along the direction of dipole moment of the water molecule).

 \vec{P} – Unit vector connecting the two Hydrogen atoms.

 \overrightarrow{Q} – Unit vector perpendicular to the plane of the Oxygen and Hydrogen atoms.

Procedure for calculation of the RMSD is provided in the Methods section. Fig. 5 (b-d) depicts the RMSD of water molecules for the three mutually perpendicular axes of the water molecules.

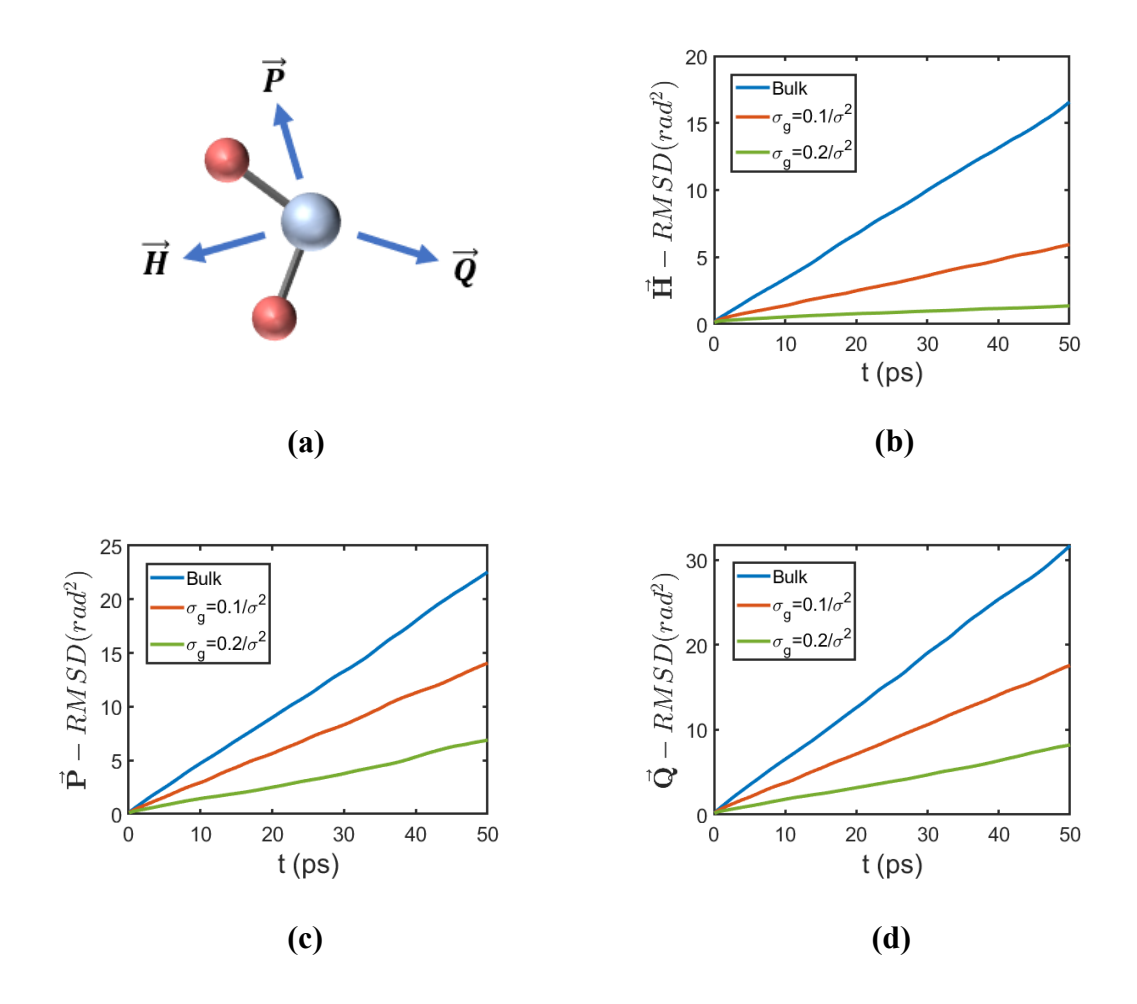


Figure 5: (a) Schematic depicting the various axes of rotation for a water molecule. (b) \vec{H} -RMSD, (c) \vec{P} -RMSD and (d) \vec{Q} -RMSD of water molecules in bulk and within the PE brush layer (for different grafting densities).

We observe a decrease in RMSD of all three axes inside the brushes in comparison to bulk water. Moreover, the RMSD decreases with an increase in the grafting density. Fascinatingly, this is different from the behavior reported by Han¹⁴ for conventional "water-in-salt" systems. In our previous study, we hypothesized that within the densely grafted PE brush layer, the structure of the brush supported counterions and water molecules, along with the charged functional groups of the PE brushes, resembled that of the "water-in-salt" electrolyte system. The PE-repeating-unitcounterion complex served as the "salt" in this system with the PE repeating units acting as the anions and the Na⁺ counterions acting as the cations. Therefore, this difference in the RMSD behavior between our case and that of Han¹⁴ is fascinating. Han¹⁴ observed a monotonic decrease in the rotational diffusivity (and thereby the RMSD) of \vec{H} with an increase in salt concentration. However, he witnessed that the rotational diffusivities of \vec{P} and \vec{Q} initially decreased and then increased with an increase in the salt concentration. Han explained that the decrease in \vec{H} -RMSD is a consequence of the enhanced electrostatic interactions between the Oxygen atoms of the water molecules (O_{Water}) and the salt cations. This is also witnessed in our system. An increase in grafting density corresponds to an increase in "salt" ("salt" as defined above) concentration within the brushes. Thus, there is an increase in Na⁺-O_{Water} interactions and the RMSD of \vec{H} decreases. Now, we take a look at the results for RMSD of \vec{P} and \vec{Q} . Han¹⁴ pointed out that the rotational motion of \overrightarrow{P} and \overrightarrow{Q} are dictated by the HBs formed by the water molecules with anions as a HB donor. An initial increase in salt concentration leads to enhanced water-anion interactions through HBs and thus decreases the rotational diffusivity of \vec{P} and \vec{Q} . However, at higher salt concentrations, the energy barrier for the rotation of water molecules decreases significantly (since there are more anions surrounding the water molecules, which makes it easier to switch between water-anion HBs), resulting in an eventual increase in the rotational motions of \vec{P} and \vec{Q} . This explained the

non-monotonic behavior of rotational diffusivity of \vec{P} and \vec{Q} in conventional "water-in-salt" electrolyte systems. We, however, observe a monotonic decrease in RMSD of \vec{P} and \vec{Q} from bulk water to sparser brushes to denser brushes (i.e., with an increase in the "salt" concentration). This indicates that there are some inherent differences between the rotational dynamics of water molecules in conventional "water-in-salt" systems and PE brush-induced "water-in-salt" systems. The rest of this article will focus on explaining how the hydrogen bonding plays a key role in dictating these vastly different orientational properties of water molecules between the two systems. We have already seen that the H_{Water} - $O_{Carboxylate}$ (H_{Water} refers to the Hydrogen atoms of water molecules) HBs or water-PE HBs are stronger than the water-water HBs (see Table 1), at least in part due to the severely restricted mobility of the PE functional groups. To investigate this further we plot the autocorrelation function for the decay of water-water and water-PE HBs inside the brushes (for $\sigma_g = 0.1/\sigma^2$) in Fig. 6. This autocorrelation function, which captures the slow HB dynamics and defines the conditional probability of existence of a HB at a time t, given that it was formed at t=0 (irrespective of its existence at intermediate times), 32 can be expressed as:

$$C_{HB}(t) = \frac{\langle h(t)h(0) \rangle}{\langle h \rangle},$$
 (1)

where h(t) = 1 if the HB exists at a time t while h(t) = 0 if it does not exist at time t. The angular brackets denote average over an ensemble of water molecules.

We observe that the water-PE HBs decay much slower (resulting in a higher average lifetime) than the water-water HBs inside the PE brushes [this was found to be true for brushes with $\sigma_g = 0.2/\sigma^2$ as well; see Fig. S6 in section S4 of the SI]. Thus, our findings reveal that the water-PE HBs are much more stable than their water-water counterparts, as quantified by their higher bond strength (energetics) as well as higher average lifetime (dynamics).

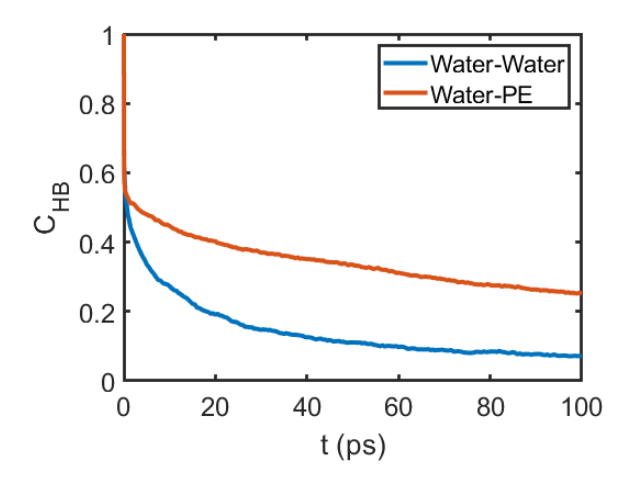


Figure 6: Autocorrelation function (C_{HB}) for water-water and water-PE HBs inside the PE brush layer with $\sigma_g=0.1/\sigma^2$.

The number of water-PE HBs per water molecule ($\bar{n}_{\text{HB, Water-PE}}$) inside the brushes increases with an increase in the grafting density (see Fig. 7). Note that this is different from the number of water-PE HBs per O_{Carboxylate} atom. In our previous paper, ¹⁰ we have indeed observed a decrease in the number of water-PE HBs per O_{Carboxylate} atom and this observation is in agreement with the findings of Szleifer et al¹² and Dahal et al^{46,47} for the case of water-swollen PEO brushes. It is the increase in the number of water-PE HBs (per water molecule) that results in the progressive decrease in RMSD of \vec{P} and \vec{Q} of the water molecules from bulk to within the sparsely grafted to densely grafted brushes (increasing "salt" concentration). Unlike the case of conventional "waterin-salt" systems, the water molecules cannot easily switch HBs from one anion (PE repeating unit) to another. The reason for this is twofold. First, there is a much higher energy barrier associated with switching due to the high stability of water-PE HBs (as explained before). Second, due to the connectivity of the PE chain, the carboxylate functional groups are arranged in a periodic fashion. Thus, there is a lower probability of two functional groups being in the immediate vicinity of a water molecule simultaneously. This too reduces the probability for switching of water-PE HBs from O_{Carboxylate} atom on one functional group to another. Thus, an increase in the number of water-PE HBs (per water molecule) at higher degrees of brush-induced confinement enforces a reduced average orientational mobility of the water molecules (due to the difficulty in switching the water-PE HBs as explained above), thereby reducing the RMSD of \vec{P} and \vec{Q} . This shows that despite the numerous similarities between the PE brush-induced "water-in-salt" electrolytes and conventional "water-in-salt" electrolytes, 9-10 these systems can show remarkably different dynamics due to the PE brush-induced spatial nanoconfinement.

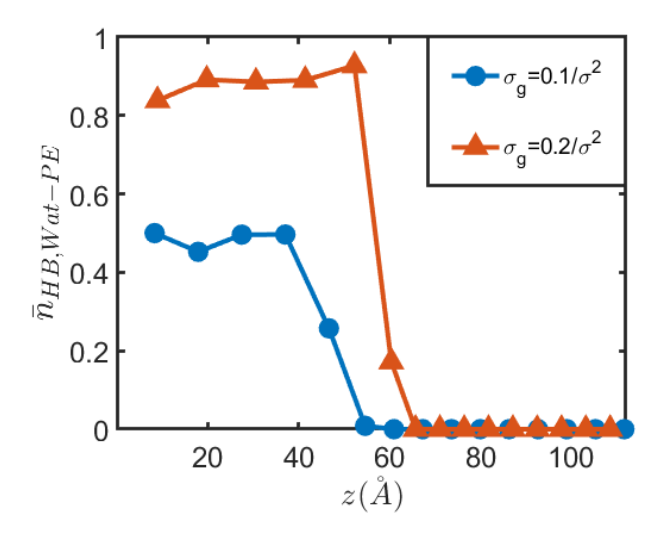


Figure 7: Transverse distribution of the number of water-PE hydrogen bonds per unit water molecule ($\bar{n}_{HB, \text{Water-PE}}$) inside the brushes for different grafting densities.

Conclusions

Through this study, we shed light on some of the most fundamental properties of water molecules, namely its hydrogen bonding and orientational dynamics inside the hydrophilic, PE-brushinduced, soft, and active nanoconfinement. First, we show that there is a reduction in the strength of water-water and water-PE HBs at higher degrees of brush-induced nanoconfinement (from bulk to sparsely grafted to densely grafted brushes). Our ring structure analysis shows that the weakening of water-water HBs is a consequence of the disruption of the extended network of water molecules inside the PE brushes. Second, the connectivity of the PE chains in addition to the stable nature of the water-PE HBs (due to a lower entropy loss associated with the formation of these HBs) result in slowing down of the orientational dynamics of all three principal axes of the water molecules with an increase in the degree of brush-induced confinement. This is a phenomenon that is not observed in conventional "water-in-salt" systems. This difference is especially important given our recent findings that inside a densely grafted PE brush layer, the structure of brushsupported water molecules and counterions, along with the charged functional group of the PE brush, resembles that of a conventional "water-in-salt" electrolyte system. It is critical to note that PE brushes are representative of a broader class of soft and active confinement, a topic that continues to elude the scientific community till date due to its highly complex nature. Thus, our findings are an important piece of the puzzle in the quest for understanding the role of spatial confinement on the structure and dynamics of soft and active nano-systems. Moreover, our results on the rotational dynamics of water molecules inside the densely grafted PE brushes can be useful for the design of novel polymer/PE based "water-in-salt" electrolytes for the next generation of Li-ion batteries with improved electrochemical properties.

In the future, we plan to extend this work by exploring several important properties of experimental significance such as the ion and water mobility, width of the hydration and counterion association layers, ion partitioning effect, etc. In addition, we shall work on refining the force field parameters for our PE brush-counterion-water system.

Methods

Molecular Dynamics Simulations

All simulations were performed on the molecular dynamics (MD) engine LAMMPS (Large Scale Atomic/Molecular Massively Parallel Simulator). As 36 fully ionized polyacrylic acid (PAA) chains were grafted on a planar surface (we refer to this plane as z=0) in a 6 x 6 square array. Each chain was N=49 backbone Carbon atoms long. Two different grafting densities ($\sigma_g = 0.1/\sigma^2$, $0.2/\sigma^2$ where σ is the Lennard-Jones distance parameter for the backbone Carbon atoms of the PAA chains) of the brushes were probed by varying the interchain separation, $\ell = 1/\sqrt{\sigma_g}$. 864 Na⁺ counterions were added to the system to neutralize the charge on the PE chains. SPC/E water molecules were added to act as an explicit solvent for the brushes. Enough water molecules were added to ensure that the height of the simulation domain was at least 1.5N σ (to eliminate any finite size effects). Two atomistic monolayers (with atoms arranged in a face centered cubic lattice with a lattice constant of 3.612 Å) were placed at the top and bottom of the simulation domain. These atoms acted as repulsive walls, preventing the mobile species (like water and Na⁺ counterions) from leaving the simulation domain. The wall atoms (top and bottom) were fixed in the x and y directions but allowed to translate as rigid bodies in the z-direction.

The OPLS-AA force field was used to model the interaction parameters for the PAA chains.⁴⁹ The bonded (bonds, angles, dihedrals and impropers) and non-bonded (Lennard Jones parameters and partial charges) parameters for the various atom types on the PAA chains were taken from the OPLS database. A comprehensive list of the force field parameters is provided in section S1 of the SI. The Lennard Jones (LJ) parameters for the Na⁺ counterions were taken from the work of Joung and Cheatham.⁵⁰ Geometric mixing rules were used for calculating the LJ

interactions between different atom types. The only exception to this mixing rule was the interactions between the Oxygen atoms of water molecules and Na⁺ counterions, which followed Lorentz-Berthelot mixing rules to be consistent with Ref. 50. The LJ interactions were calculated using a shifted truncated 12-6 Lennard Jones potential with a cutoff of 13 Å. Bonds and angles of the water molecules were constrained using the SHAKE algorithm.⁵¹ Periodic boundary conditions were used in the x and y directions, while fixed boundary conditions were used in the z direction (direction perpendicular to the grafting surface). A particle-particle particle-mesh (PPPM) solver was used to calculate the long-range Coulombic interactions between the atoms.⁵²

Our initial configuration involved a set of fully extended PAA chains (in the state of minimum entropy) with the Na⁺ counterions arranged in a straight line next to them. Water molecules were placed throughout the simulation domain (both inside and outside the brushes). The simulation was first run in a NP_zT ensemble (where the subscript z indicates that only the height of the simulation domain is allowed to change to maintain the pressure) to obtain the correct height of the simulation domain. The pressure and temperature of the system were maintained at 1 atm and 300 K respectively by using a Nosé-Hoover barostat and thermostat (with a time constant of 1 ps and 0.1 ps for pressure and temperature respectively). 53-54 Subsequently, the system was equilibrated in the NVT ensemble. The PAA chains and the mobile species (water and Na⁺ counterions) were maintained at 300 K by separate Langevin thermostats with a time constant of 0.1 ps.55 The average brush height of the system was constantly monitored to check for equilibration (see section S2 of the SI for autocorrelation function of the average end-point brush height during the production run). Following equilibration, a production run was carried out for 2 ns. Particle trajectories were calculated using the velocity Verlet algorithm with a time step of 2 fs. Positions of all the atoms in the system were dumped every 1 ps, while the positions of the PAA

atoms, Na⁺ counterions and water were dumped in separate files every 200 fs. OVITO was used for visualization of the particles.⁵⁶

Hydrogen Bond Strength Calculation

According to Ref. 16, the random joint probability distribution $[P_{rand}(r,\theta)]$ is calculated as:

$$P_{rand}(r,\theta) = 4\pi r^2 P_{rand}(\theta), \qquad (2)$$

where $P_{rand}(\theta)$ is the angular distribution associated with the donor Hydrogen-(donor Oxygen)(acceptor Oxygen) triads. Distributions of $P_{rand}(\theta)$ as well as the contours of $P_{rand}(r,\theta)$ for
water-water and water-PE donor-acceptor pairs at different degrees of brush-induced confinement
are plotted in Fig. S3 of the SI. From Fig. S3, we observe that $P_{rand}(\theta)$ [and hence $P_{rand}(r,\theta)$]
only depends on the donor-acceptor combination (water-water or water-PE) and remains almost
invariant of the grafting density of the brushes.

 $P(r,\theta)$ is the joint probability distribution in r and θ associated with an ensemble of donor-acceptor pairs at equilibrium. Both, $P(r,\theta)$ and $P_{rand}(r,\theta)$ were calculated for a maximum cutoff distance of r=10 Å between the donor and acceptor Oxygens (for both water-water and water-PE pairs). Using the methodology of Sapir and Harriers¹⁶, we calculated the potential of mean force (PMF) for the geometric phase space as:

$$PMF(r,\theta) = -RTln\left(\frac{P(r,\theta)}{P_{rand}(r,\theta)}\right),$$
 (3)

where R=8.3145 x 10⁻³ kJ/mol/K is the Universal gas constant and T=300 K is the temperature. The PMF for donor-acceptor pairs (water-water and water-PE) at different brush grafting densities are plotted in Fig. S4 of the SI.

Next, the weighted PMF $[P(r,\theta)]$ PMF (r,θ) was calculated to determine the cutoffs for the hydrogen bond formation. Fig. S5 of the SI depicts the weighted PMF for water-water and water-PE donor-acceptor pairs for different brush grafting densities.

Next, the cutoffs for hydrogen bond formation [r_1 (minimum cutoff) and r_2 (maximum cutoff)] were chosen according to the criteria: $P(r_i, \theta)$. PMF(r_i, θ)~0 as θ ~0 (i=1,2). Table S7 of the SI lists the cutoffs for hydrogen bond formation for the water-water and water-PE HBs at various degrees of brush-induced confinement.

Finally, the hydrogen bond strength ($|\Delta G|$) was determined by calculating the following double integral¹⁶:

$$\Delta G = -RT \int_{r_1}^{r_2} \int_0^{\pi} KP(r,\theta) ln \left(\frac{KP(r,\theta)}{K_{rand} P_{rand}(r,\theta)} \right) dr d\theta , \qquad (4)$$

where,

$$K = \frac{1}{\int_{r_1}^{r_2} \int_0^{\pi} P(r,\theta) dr d\theta},$$
 (5)

and

$$K_{rand} = \frac{1}{\int_{r_1}^{r_2} \int_0^{\pi} P_{rand}(r, \theta) dr d\theta}.$$
 (6)

We obtain a bulk water-water hydrogen bond strength of ΔG =-3.27 kJ/mol. This value is good agreement to the bulk water-water hydrogen bond strength of ΔG =-3.70 kJ/mol obtained in Ref. 16. The difference between the two values can be attributed to the use of different water models – Ref. 16 used TIP4Pew water model⁵⁷ while we use the SPC/E water model¹⁵. To verify this, we simulated a box of 2000 TIP4Pew water molecules under the NPT ensemble (with the temperature and pressure fixed at 298 K and 1 atm respectively) and recovered the exact value for bulk waterwater hydrogen bond strength obtained in Ref. 16 (ΔG =-3.70 kJ/mol).

Ring Structure Analysis

The ring analysis involves counting of the ring-like structures (closed loops) formed by the water molecules. This was done by following the procedure outlined in Martelli et al.24 We mapped (and stored) the HB network formed by the water molecules in our simulation domain by following the geometric criterion mentioned in Ref. 14 (r < 3.5 Å and $\theta < 30^{\circ}$). A slab of thickness 1 nm (in the z direction or the direction perpendicular to the grafting surface) was selected from within the simulation domain for the purpose of the analysis. The z-location of the slab was chosen at the center of the PE brush layer (to avoid any interfacial effects) to probe the water structure inside the brushes. On the other hand, the z-location for the slab was chosen far away from the brushes for probing the ring structure of bulk water. All the water molecules within this slab were tagged. We randomly picked one of the tagged water molecules as our starting point and iterated recursively to obtain all possible paths (a path refers to a sequential chain of molecules connected via HBs) initiating from that molecule. Out of these paths, the paths forming closed loops (involving the starting water molecule) of 10 members or less were filtered out and other paths were discarded. This was done as we considered a maximum ring size of 10 molecules for our analysis. Rings formed across the x and y periodic boundaries were considered by replicating the simulation domain in these directions (there were a total of 8 replicas of the original simulation domain). The procedure was repeated until all tagged water molecules were picked as the starting point. This way, we obtained all the rings containing at least one of the water molecules within the slab. It is important to note that a ring can contain water molecules outside of the initially tagged molecules as the slab is not periodic in the z direction. Care was taken to ensure that none of the rings were repeated by comparing a newly found ring to the list of previously stored rings. Moreover, we only considered primitive rings in our analysis. A ring is defined as primitive when

no pair of its constituent molecules are connected by a path shorter than the path along the ring [see Fig. 3(a)].³⁶⁻³⁷ This helps to avoid the erroneous counting of rings that are merely a combination of smaller fundamental rings. The analysis was carried out for multiple time steps to ensure proper statistical sampling. Finally, we utilize the list of stored primitive rings to calculate the ring statistics such as the probability distribution, average ring size, and the number of rings normalized by the number of tagged water molecules.

Procedure for Calculating the RMSDs

The RMSD corresponding to a chosen unit vector (say \vec{r} ; for the present case $\vec{r} = \vec{H}$ or \vec{P} or \vec{Q}) is calculated by employing the procedure outlined by Mazza $et~al.^{58}$ First, we discretize time into small intervals δt . The rotation of \vec{r} in time δt can be quantified as $\delta \vec{\theta}(t_i) = \cos^{-1}(\vec{r}(t_i).\vec{r}(t_i+\delta t)) \frac{\vec{r}(t_i)\times\vec{r}(t_i+\delta t)}{|\vec{r}(t_i)\times\vec{r}(t_i+\delta t)|}$ where t_i is some initial time. The net rotation of \vec{r} in a time interval t ($t \geq \delta t$) can be calculated by integrating all the differential rotations:

$$\Delta \vec{\theta}(t) = \int_0^t \frac{\delta \vec{\theta}(t^*)}{\delta t^*} dt^*, \qquad (7)$$

Finally, we take an ensemble average across a large number of water molecules to obtain the RMSD as a function of time:

$$RMSD(t) = \frac{1}{N_w} \sum_{j=1}^{N_w} \left| \vec{\theta}_j(t_i + t) - \vec{\theta}_j(t_i) \right|^2 \Rightarrow RMSD(t) = \frac{1}{N_w} \sum_{j=1}^{N_w} \left| \Delta \vec{\theta}_j(t) \right|^2, \quad (8)$$

where the rotational displacement has been averaged over N_w water molecules.

Acknowledgement

This work was supported by the US Department of Energy Office of Science grant DE-SC0017741. The authors would like to thank Dr Peter W. Chung at the University of Maryland, College Park for providing computational resources to carry out the simulations. We also acknowledge the use of high-performance cluster Deepthought2 at the University of Maryland for analyzing the results.

Supporting Information

MD force field parameters; autocorrelation function of average end-point brush height; hydrogen bond strength calculation; and autocorrelation function for hydrogen bond decay at higher grafting density

References

- Chen, G.; Sachar, H. S.; Das, S. Efficient Electrochemomechanical Energy Conversion in Nanochannels Grafted with EndCharged Polyelectrolyte Brushes at Medium and High Salt Concentration. *Soft Matter* 2018, 14, 5246–5255.
- Sachar, H. S.; Sivasankar, V. S.; Das, S. Electrokinetic Energy Conversion in Nanochannels Grafted with pH-responsive Polyelectrolyte Brushes Modelled using Augmented Strong Stretching Theory. Soft Matter 2019, 15, 5973–5986.
- Ali, M.; Yameen, B.; Cervera, J.; Ramírez, P.; Neumann, R.; Ensinger, W.; Knoll, W.; Azzaroni, O. Layer-by-layer Assembly of Polyelectrolytes into Ionic Current Rectifying Solid-state Nanopores: Insights from Theory and Experiment. J. Am. Chem. Soc. 2010, 132, 8338–8348.
- 4. Yameen, B.; Ali, M.; Neumann, R.; Ensinger, W.; Knoll, W.; Azzaroni, O. Single Conical Nanopores Displaying pH-Tunable Rectifying Characteristics. Manipulating Ionic Transport with Zwitterionic Polymer Brushes. *J. Am. Chem. Soc.* **2009**, *131*, 2070.
- Motornov, M.; Sheparovych, R.; Lupitskyy, R.; MacWilliams, E.; Hoy, O.; Luzinov, I.;
 Minko, S. Stimuli-Responsive Colloidal Systems from Mixed Brush-Coated
 Nanoparticles. Adv. Funct. Mater. 2007, 17, 2307.

- 6. Yang, Q.; Li, L.; Zhao, F.; Han, H.; Wang, W.; Tian, Y.; Wang, Y.; Ye, Z.; Guo, X. Hollow Silica-polyelectrolyte Composite Nanoparticles for Controlled Drug Delivery. J. *Mater. Sci.* **2019**, *54*, 2552–2565.
- 7. Saraswathy, M.; Gong, S. Recent Developments in the CoDelivery of siRNA and Small Molecule Anticancer Drugs for Cancer Treatment. *Mater. Today* **2014**, *17*, 298–306.
- 8. ShamsiJazeyi, H.; Miller, C. A.; Wong, M. S.; Tour, J. M.; Verduzco, R. Polymer-coated Nanoparticles for Enhanced Oil Recovery. *J. Appl. Polym. Sci.* **2014**, *131*, 40576.
- 9. Sachar, H. S.; Pial, T. H.; Desai, P. R.; Etha, S. A.; Wang, Y.; Chung, P. W.; Das, S. Densely Grafted Polyelectrolyte Brushes Trigger "Water-in-Salt"-like Scenarios and Ultraconfinement Effect. *Matter* **2020**, *2*, 1509–1521.
- 10. Sachar, H. S.; Pial, T. H.; Chava, B. S.; Das, S. All-atom Molecular Dynamics Simulations of Weak Polyionic Brushes: Influence of Charge Density on the Properties of Polyelectrolyte Chains, Brush-supported Counterions, and Water Molecules. *Soft Matter* 2020, 16, 7808–7822.
- 11. Zhuang, P.; Dirani, A.; Glinel, K.; Jonas, A. M. Temperature Dependence of the Surface and Volume Hydrophilicity of Hydrophilic Polymer Brushes. *Langmuir* **2016**, *32*, 3433–3444.

- 12. Ren, C.-l.; Nap, R. J.; Szleifer, I. The Role of Hydrogen Bonding in Tethered Polymer Layers. J. Phys. Chem. B 2008, 112, 16238–16248.
- 13. Dormidontova, E. E. Role of Competitive PEO-Water and Water-Water Hydrogen Bonding in Aqueous Solution PEO Behavior. *Macromolecules* **2002**, *35*, 987–1001.
- 14. Han, S. Dynamic Features of Water Molecules in Superconcentrated Aqueous Electrolytes. *Sci. Rep.* **2018**, *8*, 9347.
- 15. Berendsen, H. J. C.; Grigera, J. R.; Straatsma, T. P. The Missing Term in Effective Pair Potentials. *J. Phys. Chem.* **1987**, *91*, 6269–6271.
- 16. Sapir, L.; Harries, D. Revisiting Hydrogen Bond Thermodynamics in Molecular Simulations. *J. Chem. Theory Comput.* **2017**, *13*, 2851–2857.
- 17. Waluyo, I.; Nordlund, D.; Bergmann, U.; Pettersson, L. G. M.; Nilsson, A. Increased Fraction of Weakened Hydrogen Bonds of Water in Aerosol OT Reverse Micelles. *J. Chem. Phys.* **2009**, *131*, 031103.
- 18. Jabłoński, M.; Sola, M. Influence of Confinement on Hydrogen Bond Energy. The Case of the FH···NCH Dimer. *J. Phys. Chem. A* **2010**, *114*, 10253–10260.

- 19. Venables, D. S.; Huang, K.; Schmuttenmaer, C. A. Effect of Reverse Micelle Size on the Librational Band of Confined Water and Methanol. *J. Phys. Chem. B* **2001**, *105*, 9132–9138.
- 20. Wurpel, G. W.; Müller, M. Water Confined by Lipid Bilayers: A Multiplex CARS Study. *Chem. Phys. Lett.* **2006**, *425*, 336–341.
- 21. Lipkowski, P.; Kozłowska, J.; Roztoczyńska, A.; Bartkowiak, W. Hydrogen-bonded Complexes upon Spatial Confinement: Structural and Energetic Aspects. *Phys. Chem. Chem. Phys.* **2014**, *16*, 1430–1440.
- 22. Bako, I.; Bencsura, A.; Hermannson, K.; Balint, S.; Grosz, T.; Chihaia, V.; Olah, J. Hydrogen Bond Network Topology in Liquid Water and Methanol: A Graph Theory Approach. *Phys. Chem. Chem. Phys.* **2013**, *15*, 15163–15171.
- 23. Bako, I.; Megyes, T.; Ba' lint, S.; Gro' sz, T.; Chihaia, V. Water-Methanol Mixtures: Topology of Hydrogen Bonded Network. *Phys. Chem. Chem. Phys.* **2008**, *10*, 5004–5011.
- 24. Martelli, F.; Crain, J.; Franzese, G. Network Topology in Water Nanoconfined between Phospholipid Membranes. *ACS nano* **2020**, *14*, 8616–8623.
- 25. Speedy, R. J.; Madura, J. D.; Jorgensen, W. L. Network Topology in Simulated Water. *J. Phys. Chem.* **1987**, *91*, 909.

- 26. Formanek, M.; Martelli, F. Probing the Network Topology in Network–Forming Materials: The Case of Water. *AIP Adv.* **2020**, *10*, 055205.
- 27. Kumar, P.; Franzese, G.; Buldyrev, S. V.; Stanley, H. E. Molecular Dynamics Study of Orientational Cooperativity in Water. *Phys. Rev. E* **2006**, *73*, 041505.
- 28. Schmidt, D. A.; Miki, K. Structural Correlations in Liquid Water: A New Interpretation of IR Spectroscopy. *J. Phys. Chem. A* **2007**, *111*, 10119–10122.
- 29. Errington, J. R.; Debenedetti, P. G. Relationship between Structural Order and the Anomalies of Liquid Water. *Nature* **2001**, *409*, 318–321.
- 30. Matsumoto, M.; Baba, A.; Ohmine, I. Topological Building Blocks of Hydrogen Bond Network in Water. *J. Chem. Phys.* **2007**, *127*, 134504.
- 31. Lipscomb, L. A.; Peek, M. E.; Zhou, F. X.; Bertrand, J. A.; VanDerveer, D.; Williams, L.
 D. Water Ring Structure at DNA Interfaces Hydration and Dynamics of DNA Anthracycline Complexes. *Biochemistry* 1994, 33, 3649.
- 32. Luzar, A.; Chandler, D. Hydrogen-bond Kinetics in Liquid Water. *Nature* **1996**, *379*, 55.
- 33. Starr, F. W.; Nielsen, J. K.; Stanley, H. E. Fast and Slow Dynamics of Hydrogen Bonds in Liquid Water. *Phys. Rev. Lett.* **1999**, *82*, 2294–2297.

- 34. Sharp, K. A.; Madan, B. Hydrophobic Effect, Water Structure, and Heat Capacity Changes. *J. Phys. Chem. B* **1997**, *101*, 4343–4348.
- 35. Politi, R.; Sapir, L.; Harries, D. The Impact of Polyols on Water Structure in Solution: A Computational Study. J. *Phys. Chem. A* **2009**, *113*, 7548–7555.
- 36. King, S. V. Ring Configurations in a Random Network Model of Vitreous Silica. *Nature* **1967**, *213*, 1112–1113.
- 37. Wooten, F. Structure, Odd Lines and Topological Entropy of Disorder of Amorphous Silicon. *Acta Crystallogr.*, Sect. A: Found. Crystallogr. **2002**, 58, 346–351.
- 38. Santra, B.; DiStasio, R. A., Jr.; Martelli, F.; Car, R. Local Structure Analysis in Ab Initio Liquid Water. *Mol. Phys.* **2015**, *113*, 2829–2841.
- 39. Zhang, J.; Cui, C.; Wang, P. F.; Li, Q.; Chen, L.; Han, F.; Jin, T.; Liu, S.; Choudhary, H.; Raghavan, S. R.; Eidson, N. "Water-in-salt" Polymer Electrolyte for Li-ion Batteries. *Energy Environ. Sci.* **2020**, *13*, 2878–2887.
- 40. Suo, L.; Borodin, O.; Gao, T.; Olguin, M.; Ho, J.; Fan, X.; Luo, C.; Wang, C.; Xu, K. Water-in-Salt" Electrolyte Enables High-Voltage Aqueous Lithium-Ion Chemistries. *Science* **2015**, *350*, 938–943.

- 41. Yang, C.; Chen, J.; Qing, T.; Fan, X.; Sun, W.; von Cresce, A.; Ding, M. S.; Borodin, O.; Vatamanu, J.; Schroeder, M. A.; et al. 4.0 V Aqueous Li-Ion Batteries. *Joule* **2017**, *1*, 122–132.
- 42. Yang, C.; Chen, J.; Ji, X.; Pollard, T. P.; Lü, X.; Sun, C.-J.; Hou, S.; Liu, Q.; Liu, C.; Qing, T.; et al. Aqueous Li-Ion Battery Enabled by Halogen Conversion–Intercalation Chemistry in Graphite. *Nature* **2019**, *569*, 245–250.
- 43. Andot, K.; Hynes, J. T. HCl Acid Ionization in Water: A Theoretical Molecular Modeling. *J. Mol. Liq.* **1995**, *64*, 25–37.
- 44. Ando, K.; Hynes, J. T. Molecular Mechanism of HCl Acid Ionization in Water: Ab Initio Potential Energy Surfaces and Monte Carlo Simulations. *J. Phys. Chem. B* **1997**, *101*, 10464–10478.
- 45. Bagchi, B. Water Dynamics in the Hydration Layer Around Proteins and Micelles. *Chem. Rev.* **2005**, *105*, 3197–3219.
- 46. Dahal, U. R.; Wang, Z.; Dormidontova, E. E. Hydration and Mobility of Poly(ethylene oxide) Brushes. *Macromolecules* **2017**, *50*, 6722–6732.
- 47. Dahal, U.; Wang, Z.; Dormidontova, E. E. Hydration of Spherical PEO-grafted Gold Nanoparticles: Curvature and Grafting Density Effect. *Macromolecules* **2018**, *51*, 5950–5961.

- 48. Plimpton, S. J. Fast Parallel Algorithms for Short-Range Molecular Dynamics. *J. Comput. Phys.* **1995**, *117*, 1–19.
- 49. Jorgensen, W. L.; Maxwell, D. S.; TiradoRives, J. Development and Testing of the OPLS All-Atom Force Field on Conformational Energetics and Properties of Organic Liquids. *J. Am. Chem. Soc.* **1996**, *118*, 11225–11236.
- 50. Joung, I. S.; Cheatham, T. E. Determination of Alkali and Halide Monovalent Ion Parameters for Use in Explicitly Solvated Biomolecular Simulations. *J. Phys. Chem. B* **2008**, *112*, 9020–9041.
- 51. Ryckaert, J.-P.; Ciccotti, G.; Berendsen, H. J. Numerical Integration of the Cartesian Equations of Motion of a System with Constraints: Molecular Dynamics of n-alkanes. *J. Comput. Phys.* **1977**, *23*, 327–341.
- 52. Hockney, R. W.; Eastwood, J. W.; Computer Simulations Using Particles. *mcgraw-hill*.

 New York. 1981.
- 53. Hoover, W. G. Canonical Dynamics: Equilibrium Phase-Space Distributions. *Phys. Rev. A* **1985**, *31*, 1695–1697.

- 54. Nosé, S. A Unified Formulation of the Constant Temperature Molecular Dynamics Methods. *J. Chem. Phys.* **1984**, *81*, 511–519.
- 55. Schneider, T.; Stoll, E. Molecular-dynamics Study of a Three Dimensional One-component Model for Distortive Phase Transitions. *Phys. Rev. B* **1978**, *17*, 1302–1322.
- 56. Stukowski, A. Visualization and Analysis of Atomistic Simulation Data with OVITO-the Open Visualization Tool. *Model. Simul. Mater. Sci. Eng.* **2010**, *18*, 015012.
- 57. Horn, H. W.; Swope, W. C.; Pitera, J. W.; Madura, J. D.; Dick, T. J.; Hura, G. L.; Head-Gordon, T. Development of an Improved Four-site Water Model for Biomolecular Simulations: TIP4P-Ew. *J. Chem. Phys.* **2004**, *120*, 9665–9678.
- 58. Mazza, M. G.; Giovambattista, N.; Starr, F. W.; Stanley, H. E. Relation Between Rotational and Translational Dynamic Heterogeneities in Water. *Phys. Rev. Lett.* **2006**, *96*, 057803.

Table of Contents Graphic

